Synthesis of Gold NPs-Containing Thin Films from Metal Salt Injection in Ar or Ar–NH3 DBDs

Alexandre Perdrau, Noémi Barros, Rocío Rincón, Hervé Glénat, Stéphanie Truong, Sarra Gam Derouich, Xiaonan Sun, Philippe Decorse, Sophie Nowak, Béatrice Plujat, et al.

▶ **To cite this version:**

Alexandre Perdrau, Noémi Barros, Rocío Rincón, Hervé Glénat, Stéphanie Truong, et al.. Synthesis of Gold NPs-Containing Thin Films from Metal Salt Injection in Ar or Ar–NH3 DBDs. Plasma Chemistry and Plasma Processing, 2023, 43 (6), pp.1749-1772. 10.1007/s11090-023-10400-4 . hal-04396303

HAL Id: hal-04396303
https://hal.science/hal-04396303

Submitted on 15 Jan 2024

HAL is a multi-disciplinary open access archive for the deposit and dissemination of scientific research documents, whether they are published or not. The documents may come from teaching and research institutions in France or abroad, or from public or private research centers.

L'archive ouverte pluridisciplinaire **HAL**, est destinée au dépôt et à la diffusion de documents scientifiques de niveau recherche, publiés ou non, émanant des établissements d'enseignement et de recherche français ou étrangers, des laboratoires publics ou privés.

Publisher version with DOI : https://doi.org/10.1007/s11090-023-10400-4

Synthesis of gold NPs-containing thin films from metal salt injection in Ar or Ar-NH_3 DBDs

Alexandre Perdrau[1,2], Noemi Barros[1,2], Rocio Rincon[1,3], Hervé Glénat[1], Stéphanie Truong[4], Sarra Gam Derouich[4], Xiaonan Sun[4], Philippe Decorse[4], Sophie Nowak[4], Beatrice Plujat[1,2], Souad Ammar[4], Jean Pascal Borra[5], Fiorenza Fanelli[6], Françoise Massines[1]

[1] Laboratoire Procédés Matériaux et Énergie Solaire (PROMES, CNRS), UPR-8521, Rambla de la thermodynamique, FR-66100 Perpignan, France
[2] Université Perpignan Via Domitia (UPVD), 52 Av Paul Alduy, FR-66100 Perpignan, France
[3] Laboratory of Innovation in Plasmas (LIPs), Universidad de Córdoba, 14071 Córdoba, Spain
[4] Laboratoire Interface Traitement Organisation et Dynamique des Systèmes (ITODYS), Université Paris Cité, CNRS, UMR-7086, 15 rue Jean-Antoine de Baïf, FR-75205 Paris, France
[5] Laboratoire de Physique des Gaz et des Plasmas, (LPGP CNRS-Université Paris-Saclay), UMR-8578, Bat 210, rue Becquerel, Université Paris-Saclay, FR-91405 Orsay Cedex, France
[6] Institute of Nanotechnology (NANOTEC), National Research Council (CNR), Bari, Italy

Abstract

This study focuses on metal/polymer nanocomposite thin films made by atmospheric pressure Plasma-Enhanced Chemical Vapor Deposition (AP-PECVD). The aerosol of isopropanol-dissolved tetrachloroauric acid ($HAuCl_4$:3H2O gold salt) is injected in a dielectric barrier discharge (DBD) to synthesize plasmonic nanocomposite thin films. Argon is used as carrier gas with or without 133 ppm addition of ammonia (NH_3) to respectively get or not a Penning mixture. Results show that NH_3 largely influences the salt reduction and thin film properties.

According to the aerosol characterization, the size distribution at the plasma entrance supports that isopropanol mainly evaporates before injection in the plasma. The salt initially dissolved in each droplet precipitates during evaporation before injection as solid nanoparticles of about 30 nm diameter with eventual traces of solvent. Then, the nanocomposite thins film are studied. Optical properties, as plasmonic resonance, are characterized by UV-visible absorption spectroscopy. The chemical composition is analyzed using X-ray photoelectron spectroscopy (XPS) and Raman spectroscopy, complemented by X-ray diffraction (XRD) analysis as well as chemical mapping obtained by Energy dispersive spectroscopy (EDS) coupled to scanning electron microscopy (SEM) operating in Scanning Transmission Electron Microscopy (STEM) mode. Additionally, the morphology of the deposits is investigated by atomic force microscopy (AFM) and SEM, highlighting the influence of NH_3 gas on the film nature and therefore its role in the overall deposition process. Finally, optical emission spectroscopy (OES) of the plasma gives clue to better understand the effect of NH_3.

The overall results show that the salt nanoparticles are reduced in the plasma phase leading to non-aggregated metal Au NPs embedded in a carbon-based matrix formed by isopropanol polymerization. The presence of NH_3 in the plasma unambiguously decreases the salt reduction and affects the thin film properties, consequently changing their plasmonic response related to the size, concentration and composition of the embedded NPs.

1 Introduction

Due to their robustness and ease of use, dielectric barrier discharges (DBDs) have been widely studied and used since they were discovered by Siemens. For decades, U. Kogelschatz[1] largely participated in their developments in various fields. Specifically, DBDs have found applications in material science for surface functionalization [2] or the synthesis and deposition of thin films for solar cells[3], [4], in foam[5] or as water barriers[6] as examples. Among other low-temperature plasma sources, DBDs are distinguished for their capability to achieve high-quality plasma deposition of dense films at atmospheric pressure. In the corona configuration, they allow in-line treatment of large surface[7]. Depending on the gas chemical composition, the voltage frequency, the nature of the dielectrics and the configuration, DBDs can be divided into two families defined by the gas breakdown mechanism: streamer breakdown leading to filamentary DBD or Townsend breakdown leading to diffuse DBD[1], [8], [9]. The first one leads to the development of microdischarges having a radius of about 100 µm which last less than 100 ns[10], whereas the second one produces glow or Townsend diffuse discharges[11], [12]. The use of a Penning mixture such as Ar/NH_3 favors the formation of diffuse DBDs[13], [14], thanks to a good adequation between the energy of metastable states of the carrier gas (Ar, ~11.5 eV) with the ionization potential of an impurity (NH_3, ~10.1 eV) giving place to Penning ionization due to the collision of a metastable excited state of the carrier gas with other species.

More recently, DBDs have been used for the synthesis of nanocomposite (NC) thin films[15] by atmospheric pressure plasma enhanced chemical vapor deposition (AP-PECVD). A NC thin film is a matrix in which particles ranging from few to hundreds nanometers, called nanoparticles (NPs), are embedded[16]. Depending on the nature of the NPs, thin film properties can differ[17]. For instance, when metal NPs are used, the NC can have a plasmonic response[18]–[20]. Plasmons are collective oscillations of free electrons in metal NPs and these oscillations are at their maximum when the frequency of the incident wave to which the NPs are subjected corresponds to the electron oscillation frequency. This phenomenon is called surface plasmon resonance. Gold NPs are of special interest due to their appealing optical properties[21]. For instance, they are promising in the field of solar energy, particularly in the development of photovoltaic panels[22] since plasmon resonance occurs at wavelengths aligned with a zone of high emission in the solar spectrum.

Different solutions were explored for synthesizing NC thin films on large surface areas using DBDs. For the sake of simplicity, most of them use an aerosol, *i.e.* droplets of the thin film precursors transported by a carrier gas to the plasma. The first approach consists of injecting into the DBD a solution of premade NPs in suspension in a polymerizable solvent[15], [23], [24]. Although this route allows for a large variety of nano-objects to be injected into the discharge favoring the synthesis of complex multifunctional NC materials, NPs are found as aggregates when the solvent evaporates[24]. Even if NCs containing NP aggregates could be of interest when large surfaces of interaction are required, *e.g.* in photocatalysis for water treatment[25], NP aggregation could be avoided by NP functionalization[26] or by forming the NPs in the gas stream before the plasma or in the plasma which avoids hazardous chemicals manipulation. The second approach is based on the in-situ synthesis of NP from, as an example, a metal precursor, such as a metal salt[27], and their incorporation inside a polymer matrix[28].

Depending on the frequency applied to the plasma, the mechanisms taking place in the discharge differ, in turn affecting thin film properties. Despite that at low frequencies of about 1 kHz, the discharge power is too low to polymerize the matrix precursor[29], it can induce a drift of NPs to the surface via the Coulomb force if the NP diameter reaches 10 nm and NPs achieve a fixed charge[30]. At higher frequencies (above 10 kHz), the discharge power increases promoting a higher solvent polymerization[7]. Therefore, alternating low and high frequency, *i.e.* provoking a modulation of the plasma, makes it possible to control the morphology of the NC obtaining homogeneous thin films[31]. This plasma-modulation approach has been successfully utilized for the synthesis of TiO_2/SiO_2 NCs from TiO_2 NPs in hexamethyldisiloxane (HMDSO)[26], NC formation based on TiO_2 NPs embedded in a carbon-based matrix from TiO_2 NPs dispersed in isopropanol (isopropyl alcohol, IPA)[24] or, more recently, SiO_2-based NCs in a biodegradable polymer from SiO_2 NPs dissolved in ethyl lactate (ELA)[32]. Lately, this approach was also utilized for the formation of Au NPs based NCs[27]. Nadal et.*al.*[27] injected directly into the Ar plasma a metal salt ($HAuCl_4$) dissolved in a polymerizable solvent, namely isoproponal in the form of an aerosol leading to the simple in-situ synthesis of a metal/polymer NC with non-aggregated gold NPs.

The novel venue reported in [27] demonstrated the potential of DBDs in the one-step and safe-by-design process for the synthesis of Au NCs. Nevertheless, for large-scale production, the process must be optimized in terms of, for example, carrier gas selection. In this research, the effect of using both Ar and Ar/NH_3 as Penning mixture for NCs formation is deeply studied. Optical emission spectroscopy was utilized for understanding the gold salt reduction process and different material characterization techniques revealed the role of the carrier gas on the optical properties, chemical composition, structure and morphology of the deposited gold/polymer NCs thin films.

2 Experimental details

2.1 AP-PECVD set-up

Figure 1 shows a schematic representation of the experimental set-up. Solutions of gold salt ($HAuCl_4 \cdot 3H_2O$, 99.99% pure, Aldrich) dissolved in reagent grade isopropanol at 0.1 gold weight percent (% of gold mass in the mixture) are first prepared. A liquid aerosol of the solution is then produced by pneumatic fragmentation of liquid meniscus with impaction of bigger droplets to remove them in a TSI® constant output liquid atomizer. The temperature of the solution is controlled by a thermostatic bath, and its weight is measured at the beginning and at the end of each experiment to determine the mass flow rate of atomized solution (expressed in g/min) injected in the plasma during the deposition process. To reduce the amount of atomized thin film precursors, the Ar gas flow rate used to produce the aerosol is set to the minimum value ensuring a continuous droplet production by the atomizer: 0.9 L/min. Pure Ar or Ar/NH_3 mixture is added at the flow rate of 3.1 L/min to the aerosol stream to dilute thin film precursors concentration before the plasma inlet. Consequently, the aerosol droplets are transported in a 4 L/min carrier gas flow with or without 133 ppm of NH_3.

The plasma reactor is composed of two parallel electrodes with 2x5 cm^2 area both covered by a 1 mm thick dielectric layer. The aerosol is injected within the 2 mm gap between the two dielectrics. Once injected, the feed mixture is guided by two quartz bars until its aspiration on the opposite side to avoid lateral precursor losses and ensure a laminar gas flow of constant velocity in the plasma. Thanks to controlled leakage, the pressure is constant and equal to 760 Torr. The mean gas residence time in the plasma zone is 30 ms. Deposition is performed during 40 min on circular glass substrates (diameter of 22 mm and thickness of 0.2 mm, Oxford Instruments) placed on the lower dielectric. In this study, the thin film characterization is made at 3 mm from the feed mixture entrance into the plasma zone (4.5 ms residence time).

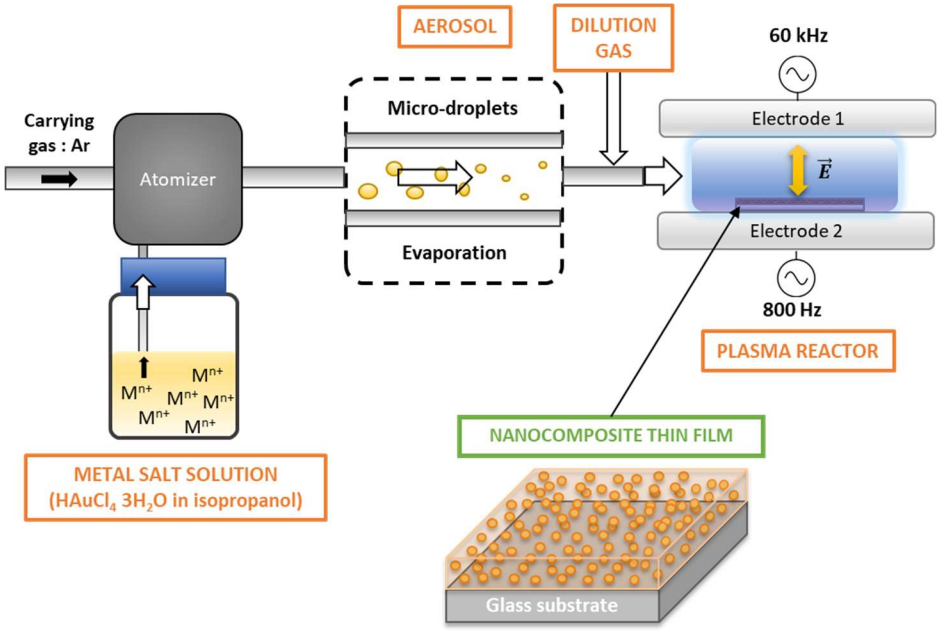

Figure 1: Global view of the NC thin film AP-PECVD set-up, in which a metal salt solution is atomized by using an Ar flow and the resultant aerosol is diluted and injected inside the plasma chamber.

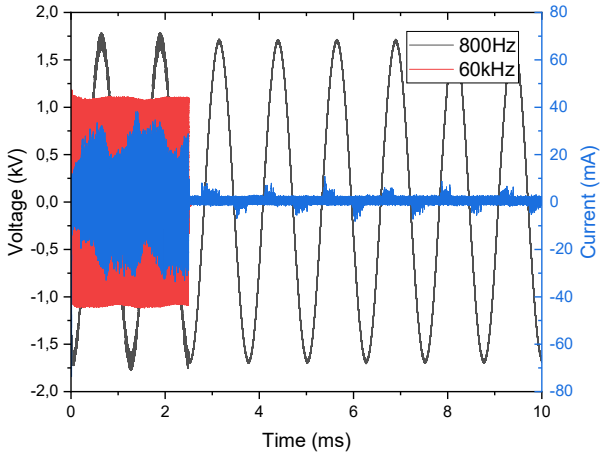

Figure 2 : Low (black) and high (red) frequency voltages, and current (blue) measured on a complete cycle (800 Hz + 60 kHz for 2.5 ms, Duty cycle = 0.25) during NC thin film deposition.

Table 1 : Main experimental parameters used to prepare the two families of samples: A samples with NH_3 and NA samples without NH_3.

Experimental parameters/Samples	**A**	**NA**
NH_3 in the dilution flow	Yes	No
Bath temperature [°C]	20	20
Room temperature [°C]	26 ± 3	24 ± 1
Solution flow rate [g/min]	0.18 ± 0.01	0.19 ± 0.02
IPA [%]	1.8 ± 0.01	1.9 ± 0.02
Gold salt [ppm]	< 6 ppm	< 6 ppm
NH_3 [ppm]	133	0
800 Hz peak-to-peak amplitude [kV]	3.4	3.4
60 kHz peak-to-peak amplitude [kV]	2.2	2.2
60 kHz surface power density [$W \cdot cm^{-2}$]	0.11 ± 0.02	0.09 ± 0.03

As previously explained, two plasma frequencies are needed to synthesize the desired NC in a DBD[24]: (i) a frequency lower than 1 kHz to drift the NPs to the substrate (ii) a frequency higher than 10 kHz to polymerize IPA with a thin film growth rate increasing proportionally to the frequency. In the present work, the plasma is created using a superposition of a low-frequency voltage (0.8 kHz, 3.4 kV peak-to-peak amplitude) applied continuously, and a high-frequency voltage (60 kHz, 2.2 kV peak-to-peak amplitude) applied during 2.5 ms every 10 ms. According to Bazinette et al.[33], the 800 Hz voltage does not have any effect on the 60 kHz DBD. Thus, even if the 800 Hz is continuously applied, it can be considered that the DBD used in this work corresponds to alternating 800 Hz and 60 kHz discharges, with voltage amplitude of 3.4 kVpp and 2.2 kVpp, respectively. These amplitude values were chosen according to the following criteria: the high value of the low frequency voltage ensures an efficient particle transport toward the substrate. The value of the high frequency voltage is 100 V higher than the breakdown voltage and leads to a DBD power of around 0.1 W/cm^2. Each voltage is provided by a low frequency signal generator (Agilent 33220) and an audio amplifier (Crest CC4000) connected to an up-voltage transformer (Boige et Vignal or Montoux). The two voltages are synchronized and applied to different electrodes. Specifically, the upper electrode is powered by the 60 kHz voltage and the lower one by the 800 Hz voltage (Figure 2). This technical solution allows for choosing independently each frequency and each voltage amplitude, which was not possible with the so-called frequency shift keying (FSK) mode used previously[27]. Figure 2 presents the two voltages over a complete cycle and the current measured when the aerosol is injected. Both the 800 Hz and

the 60 kHz DBDs are filamentary DBDs. This is always the case in the presence of the aerosol whether or not the carrier gas contains NH_3. NH_3 addition only induces a slight increase in the discharge power (Table 1).

While NH_3 has little influence on the discharge, it has a major one on the NC thin film. Thus, two sets of operating conditions are considered in this study: a first NH_3 (A) and a second without NH_3 (NA). For each set, at least three different samples were prepared. Table 1 summarizes the experimental conditions used to prepare the two families of samples as well as the maximal amount of each chemical species entering the plasma.

2.2 Characterization techniques

2.2.1 Aerosol

Size distributions of droplets from 15 to 750 nm have been measured at several positions between the atomizer and the plasma using a differential mobility analyzer (DMA TSI 3071). For practical reason, these measurements cannot be done with Ar, but with N_2. However, similar droplet sizes are expected in both gases since the surface tension of isopropanol, controlling the size of droplets produced by pneumatic nebulization, as well as the saturation vapor pressures are very close in both Ar and N_2[34]. The gas flow rate in the atomizer is the same as the one used to deposit the NC films (0.9 L/min), while the atomized solution has a gold weight concentration (0.2 wt %) twice that used for thin film deposition.

2.2.2 Nanocomposite thin films

Optical, morphological and structural properties of the thin films as well as their chemical composition are determined using complementary techniques. When spatial resolution is available, measurements are systematically made at 3 mm from the gas inlet in the plasma zone to avoid variations related to the reactive components residence time in the plasma.

Optical properties

UV-vis absorption spectra of the films are measured on a 2 mm spot using an Ocean Optics DH-2000 lamp with a halogen and a deuterium lamp to cover the UV-vis range and an AvaSpec-ULS2048XL-EVO spectrometer from Avantes to record the spectra.

Morphological and structural properties

X-ray diffraction measurements (XRD) are carried out on an Empyrean diffractometer (Malvern-Panalytical) equipped with a copper tube (filtered radiation Kα=1.541874 Å), a sampling holder position 5-axis cradle and a PIXcel multi-channel detector. The diffractometer operates within the theta-theta Bragg-Brentano configuration in a 2θ angular range of 15° to 90° (step size and time of 0.0263° and of 160 s, respectively). The XRD data were treated and analyzed using Highscore+ (Panalytical) software.

Scanning Electron Microscopy (SEM) observations are carried out on a ZEISS Gemini SEM 360 FEG-SEM microscope, operating at 5.0 kV. The samples surface is graphitized (~10 nm in thickness) by carbon thermal evaporation to avoid charge accumulation during the observations, making intrinsic NC film carbon content analysis impossible.

The morphology of the deposits is also investigated using a commercial atomic force microscope, AFM (SMENA NT-MDT). Scans are performed in intermittent contact mode. The tips used are manufactured by NANOSENSORS with a resonance frequency of 160 kHz and a radius of curvature of the apex of less than 10 nm. Grain size analyzes were performed with a thresholding algorithm implemented in Gwyddion software. The size of the grains is defined by an equivalent radius. It corresponds to the radius of the disc having the same surface as the projected surface of the grain.

Chemical composition

The previously described SEM-FEG microscope is equipped with a Oxford Instrument energy-dispersive X-ray spectroscopy (EDX) detector (Ultim Max 170 mm^2 detector) for the elemental analysis and imaging coupled to topography imaging. EDS chemical mapping is also carried out using a Inlens SE detector (In Column) operating at 8 kV. The distance used between the sample and the EDX window was fixed to 41 mm for a working distance

of 8.5 mm and solid angle of 35°. EDX data treatment and analysis is made with the Oxford Instrument AZtec software.

X-ray photoelectron spectroscopy (XPS) analyses are performed using a K-Alpha$^+$ spectrometer (Thermo.Fisher Scientific, East Grinstead, UK) operating in the constant analyzer energy mode and equipped with a micro-focused and monochromatic Al Kα X-ray source (1486.6 eV, spot size: 400 µm, 12 kV, and 6 mA) and a flood gun (charge compensation system for insulating samples). For the analysis, the NC films are clipped onto the sample holder and outgassed 12 hours in the fast-entry lock. The pass energy is fixed to 200 eV and 40 eV for the survey and the high resolution regions, respectively. The photoelectron take-off angle was normal to the surface of the samples and the sample surface covered by each analysis is of 0.5024 mm^2 ($\pi \times 0.4^2$ mm^2). The binding energy scale is referenced to the (C-C/C-H) C 1s component at 285.0 eV. Data acquisition and processing are made using Advantage software ThermoFisher Scientific, version 5.9902. The surface chemical composition was calculated by using the manufacturer sensitivity factors.

Raman spectroscopy was used to get insights into the structural properties of the carbon matter, thanks to a high resolution Horiba HR 800 Raman microspectrometer coupled to a microscope with a 1000x long distance objective (N.A = 0.9) for experiments in air. A He−Ne laser beam operating at 633 nm is used as an excitation source. Its power is fixed to 63 µW for 1% filter and 0.5 mW for 10% filter at the sample (spot size of 200 nm in diameter). The spectra are collected in the whole 180-3000 cm^{-1} wavenumber with an acquisition time of 10 s along 3 accumulations each.

2.2.3 Plasma diagnostic by optical emission spectroscopy (OES)

Light emitted from the plasma is collected by a 600 µm optical fiber with a collimator lens which is placed perpendicularly to the gas flow direction at 3 mm from the gas entrance in the plasma zone. The light is then directed to the 25 µm width slit entrance of a Maya2000Pro spectrometer (Ocean Optics) with a 14 µm pixel size. Prolonged exposure time (1 s) optical emission spectra in the 220-1050 nm range is taken in each experimental condition to discern the effect of NH_3 in the deposition of NC thin films.

3 Aerosol characterization

Droplets produced by the atomizer are diluted 2.4 s after production by liquid fragmentation in the atomizer while they are transported by the carrier gas during 2.8 s before entering the plasma. During that time, both size and concentration evolve, due to evaporation, losses to the walls and coagulation by diffusion of NP, as well as by dilution. To determine the liquid or solid state of the aerosol injected in the plasma, size distributions have been measured at several positions between the atomizer and the plasma.

At first, measurements made with non-volatile paraffin show that with a gas flow of 0.9 L/min, the atomizer generates around 6.10^7 droplets per cm³, with a number median diameter value of 340 nm. Then, the aerosol generated from a solution of gold salt in isopropanol is investigated. After 0.4 s, the mean diameter already drops down to 40 nm, as expected from fast evaporation of isopropanol. Indeed, amorphous or crystallized salt crystal NPs can be formed depending on the ratio of the evaporation rate, controlling the formation rate of primary nuclei of solid salts by local surface precipitation in each droplet, over the diffusion rate of these primary nuclei of crystal from the surface, where they necessarily appear due to the local surface oversaturation of salt in solution by surface precipitation[35]. The dilution, done later, 2.4 s, induces an additional evaporation step and a decrease of the droplets concentration. At the entrance of the plasma reactor, the measured NPs concentration is around 10^6 per cm³, with a mean diameter of 36 nm. This value is slightly higher than the one estimated for a dry salt residue (around 32 nm, assuming a crystallized $HAuCl_4$:3H2O salt with a density of 3.9 g/cm^3 and a spherical shape of amorphous salt or/and faceted shape of salt crystal. Hence, the aerosol injected into the DBD is made of suspended solid particles slightly bigger than the dense crystallized salt NP that would have been formed by slow evaporation of all the solvent from the initial solution droplet. These small differences from 10 to 15% are observed between the measured 36 nm and the expected 32 nm mean diameters of NPs injected in the plasma assuming total solvent evaporation. Despite this difference close to 10 to 15%, measurement errors related to flow rate uncertainties of sampled and sheath gas flows in the DMA, the reproducibility of these size distributions evolution supports that NPs entering the plasma are slightly larger than expected for the perfectly crystallized salt NP that can be formed

by complete and slow evaporation conditions. This is either due to residual traces of solvent around the 30 nm solid salt core of NPs or/and to a lower density of a probably amorphous salt NPs that could be formed in such fast evaporation conditions leading to amorphous more or less spherical and porous solid particles[35].

During pneumatic fragmentation of the salt solution in the atomizer, used for the production of droplets suspended in the carrier gas, i.e. for the production of the initially liquid aerosol, evaporation of the solvent is observed and characterized by the measure of the gold salt concentration in the solution to be nebulized, before and after experiments. This evaporation increases the IPA quantity in the aerosol and is sensitive to temperature. However, the partial pressure of isopropanol is always far below the saturation vapor pressure, as demonstrated by the fast evaporation of initial 300 nm droplets down to 30-40 nm salt particles after only 0.4 s (measurements very close to the atomizer outlet). To control this parameter, the bottle containing the solution was placed in a thermostatic bath. However, as shown in Table 1, this bath is insufficient to fully stabilize the solution flow rate as the room temperature varies. Besides, this evaporation also limits to 2 h the duration of experiments to avoid the increasing salt concentration of the solution in the atomizer with subsequent larger dried NPs formed by evaporation of initial droplets with the same sizes. This effect is limited here with large volume of solutions and short experimental tests (< 2 h). It could also be handled by continuous refilling of the solution in the bottle by a solution with a controlled concentration of salt.

According to these results, with the experimental conditions used in the film deposition (solution concentration of 1.6 mg/mL, i.e. 0.1% in weight of gold), the distribution size of the NP entering the plasma should have a modal diameter around 25-30 nm. Assuming the total conversion of gold salt to metallic gold to form crystalline spherical NPs, the diameter of the gold NP should then be around 12 nm.

4 Thin film analysis

4.1 Optical properties

NCs obtained by injecting the aerosolized $HAuCl_4$ solution in a pure Ar DBD (NA) are purple, and exhibit a large absorption band between 500 and 900 nm (**Errore. L'origine riferimento non è stata trovata.**a), attributable to the plasmonic resonance of gold NPs. The width of the band might be due to a large size distribution of the NPs, or could indicate the presence of strong inter-particle interactions, as a consequence of very short inter-particle distances[36]. The shift to high wavelength could also be related to the polymer coating of the NPs. On the contrary, the NCs prepared in presence of ammonia (A) have a dark-brown color and do not evidence a net plasmonic signature in their absorption spectra (**Errore. L'origine riferimento non è stata trovata.**b).

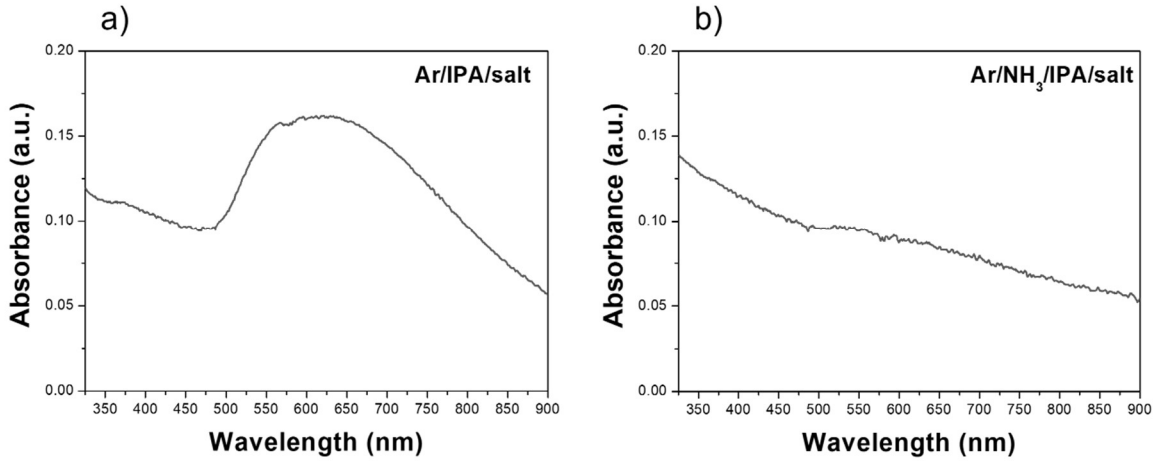

Figure 3 : UV-vis absorption spectra of a) NA and b) A samples.

4.2 Phase and morphology analysis

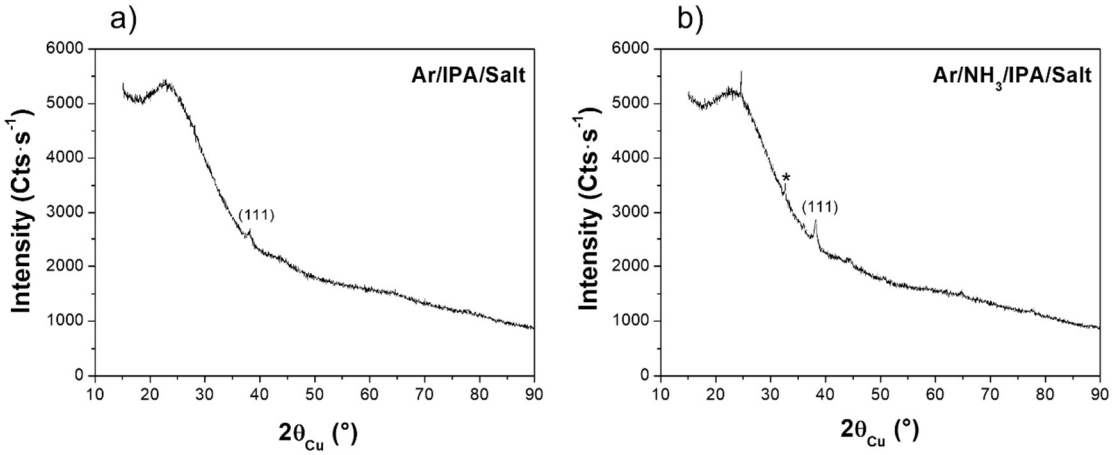

Figure 4 : XRD patterns of a) *NA and* b) *A samples*

XRD patterns recorded on NA and A samples show that gold NPs are present in both samples. The characteristic (111) Au diffraction line is clearly evidenced (ICDD N° 98-004-4362) in both samples, even if its intensity is higher in A pattern than in NA one (

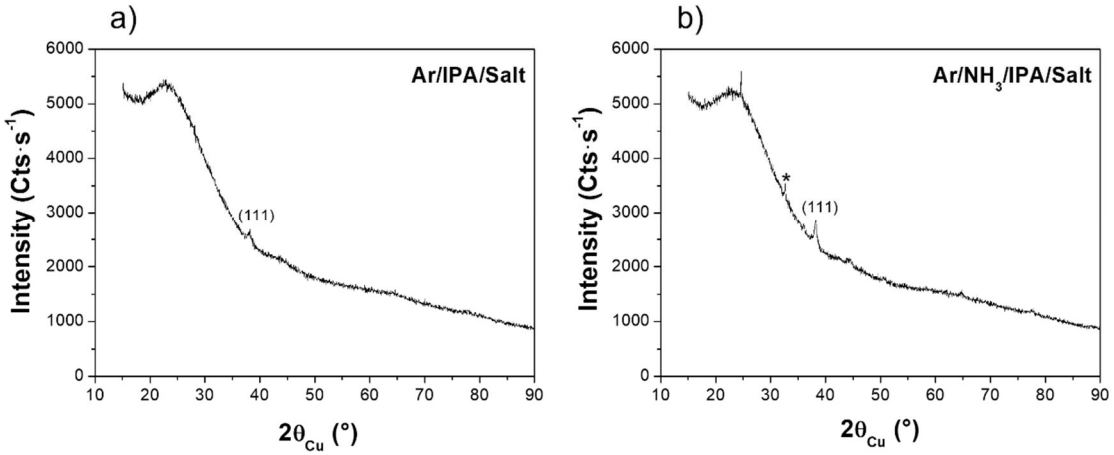

Figure 4). Typically, the pick area for NA sample is found to be equal to 318 ± 110 Cts·s^{-1}·° while it is of 486 ± 100 Cts·s^{-1}·° for A sample. Using the Scherrer equation, a crystal size can be inferred from the (111) peak broadening. Assuming isotropic in shape crystallographic coherent domains, an average value of 7.8 ± 1.8 nm and 13.1 ± 2.0 nm is measured for NA and A samples, respectively. Note that an additional weak peak is observed in the pattern of A sample which might be attributed to layered graphite (ICDD N°98-005-3781). The appearance of a single and small in intensity peak does not allow any conclusions to be drawn regarding the presence of graphite, which, however, might explain the black sample color.

The initial low-magnification SEM observations on A and NA samples (Figure 5) evidence two different morphologies. Without ammonia (NA sample), the coating is mainly made of dense non-aggregated and almost isotropic in shape NPs (Figure 5a) having a diameter about 20nm. The selected image almost shows non aggregated NPs aggregation, with a few number of clustered NPs. With ammonia, the collected images of A samples are fully different due to the presence of large rounded structures (likely large NPs) that are often surface-decorated with smaller and highly contrasted particles. These small particles appear also as individual objects as those observed for NA sample.

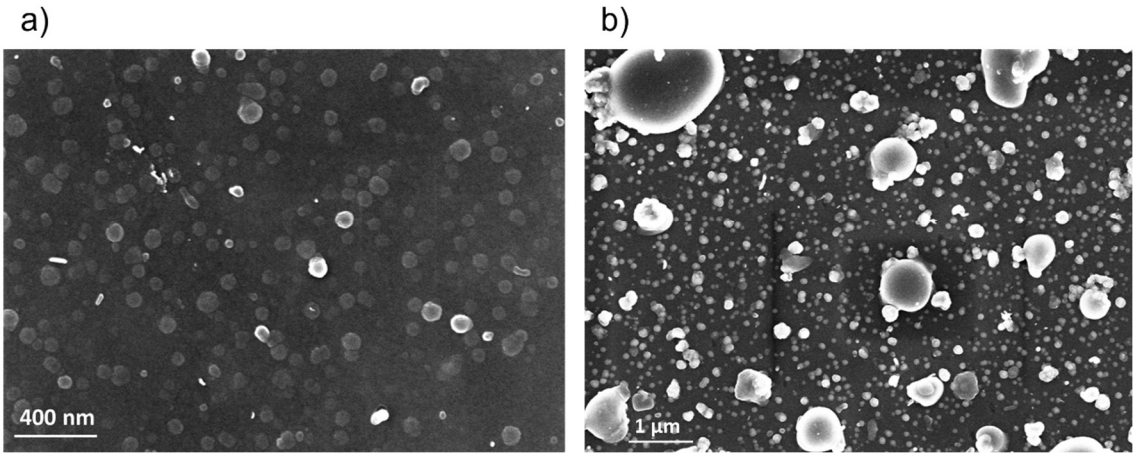

Figure 5: SEM images of a) NA sample and b) A sample.

In agreement with low-magnification SEM observations, AFM topographic scan on NA sample (without NH_3 addition) reveals a surface nanostructuration with mainly NPs, assumed to contain gold, most of the time arranged in rosaries. It should be noted that the probe convolution artifact presented in the AFM image of the NH_3-free deposit (Figure 6a) is corrected by modeling the AFM tip from the manufacturer's specifications and then by applying an image algorithm for erosion [37]. Grain size analysis shows a NPs size distribution centered around an equivalent radius of about 10 nm (6b). An attentive lecture of Figure 6b shows that in fact there is a double distribution. The main one (87% of the grains), has a mean radius of 12 ± 3 nm which could be related to non-aggregated NPs. The second one is between 15 nm and 35 nm and could correspond to assemblies of gold NPs bound by polymer, as suggested by the clearer shapes on the AFM scan in 6a. Since the adhesion of the deposits is low, a scratch test of the deposit is also carried out to assess its thickness (6c). There is a step height equivalent to the maximum height of the surface profile (S_t=35 nm). This means that the deposit is mainly formed of a discontinuous monolayer of NPs. For this coating, the presence of the polymer is difficult to be detect.

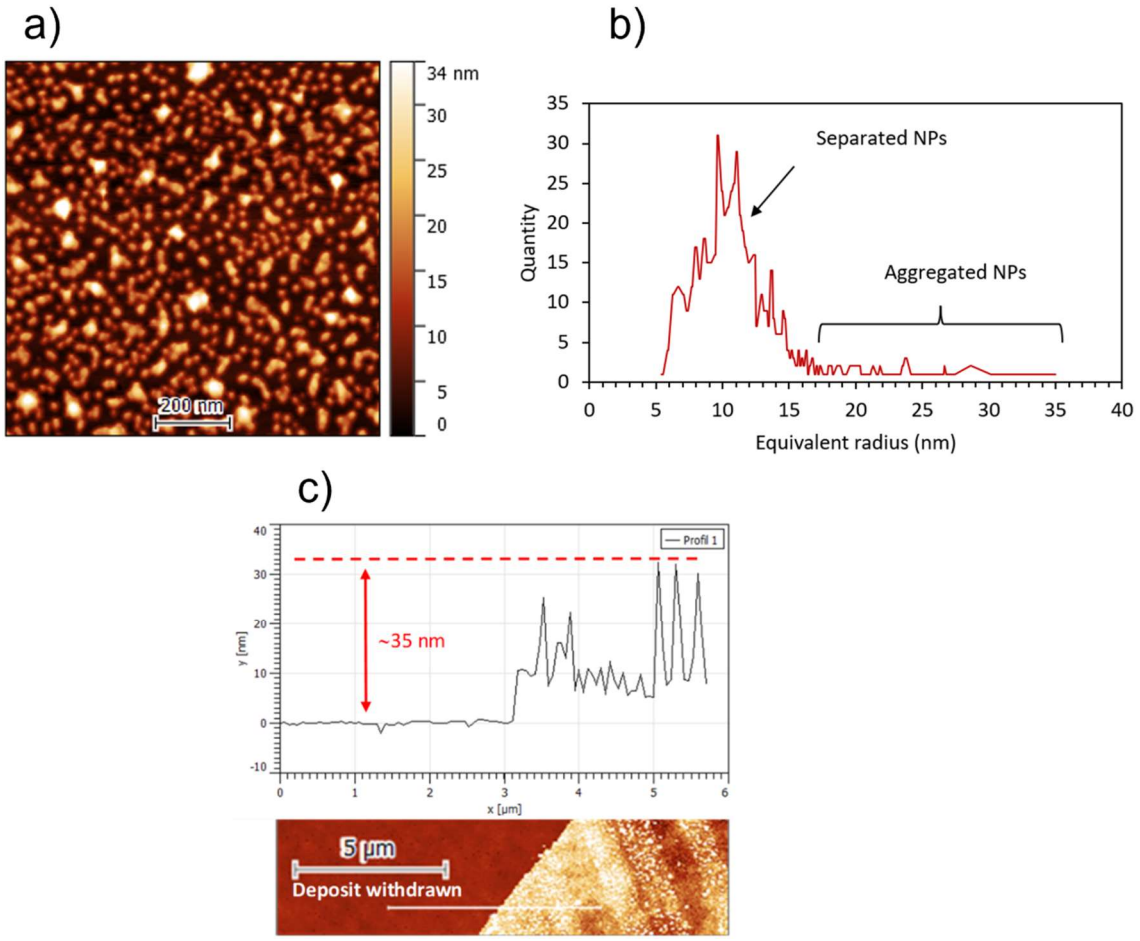

Figure 6 : AFM observation of a NA sample (without NH_3); a) topographic scans of the deposit, b) grain size distributions inferred from AFM image analysis and c) scratch test profile measured on the white line of the scratched sample image.

AFM topographic scan on an A sample (with NH_3 addition) reveals a surface nanostructuration with less dense NPs coverage (Figure 7a). The analysis of the size of the particles evidences of a larger size distribution, with equivalent radius varying between 30 nm for the smallest to 200 nm for the largest NPs (Figure 7b). These particles are systematically wider than tall with an aspect ratio of about 0.3. An average equivalent radius over the entire distribution could be nevertheless deduced with a value of 91 ± 37 nm. Coupling the topographic image to the phase signal shows particles with a faceted shape, suggesting the formation of crystals (Figure 7c). The phase image also reveals a slight heterogeneity around the particles which could be linked to the presence of a carbon-based polymer coating. The small circular spots are characteristic of the glass substrate.

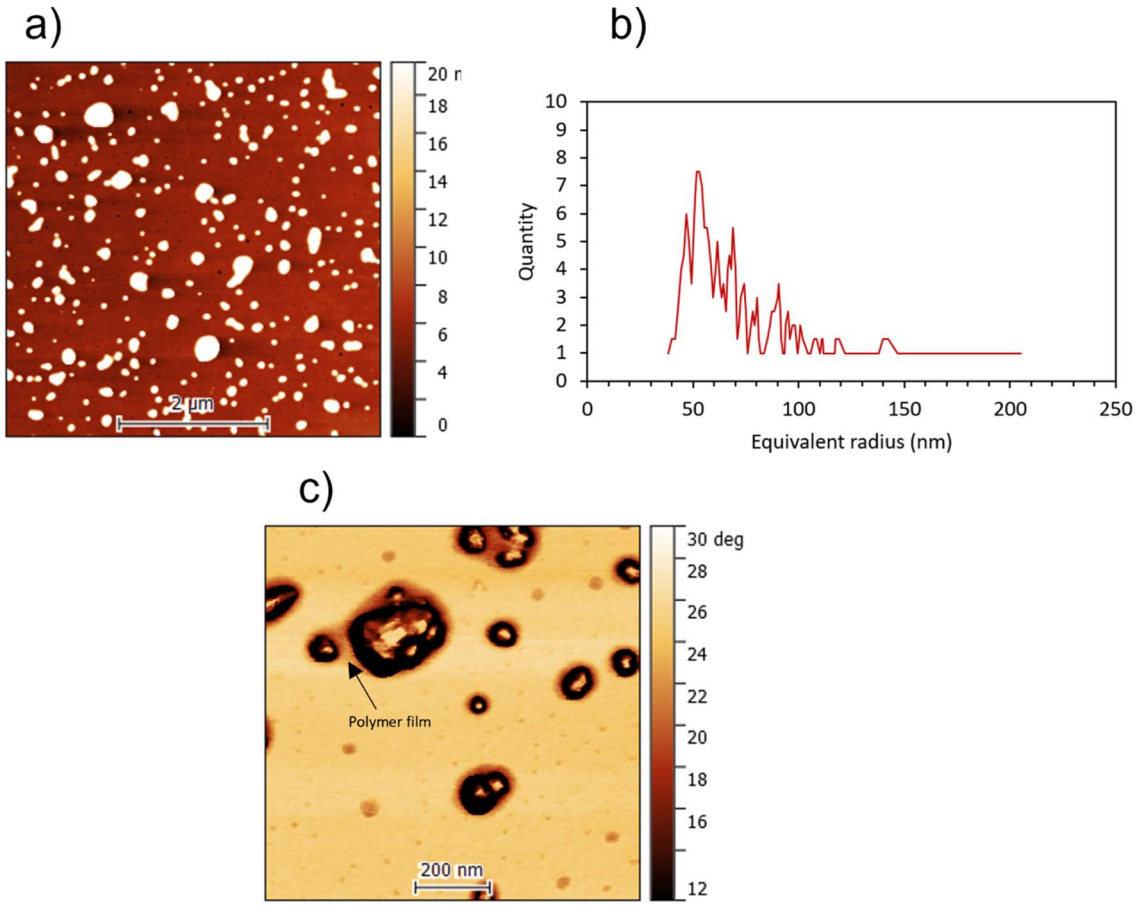

Figure 7: AFM observation of an A sample (with NH_3); a) 5x5µm² topographic scan; b) grain size distributions inferred from the AFM scan (c) 1x1µm² phase scan.

These two deposits being discontinuous, the bearing areal ratio curve extracted from the topographic scan, also called the ABBOTT curve [38], makes it possible to estimate the volume of material deposited. The calculations show a volume of material deposited approximately 1.3 times greater for the deposit without NH_3 compared to that with NH_3, respectively $9.4x10^{-3}$ $\mu m^3/\mu m^2$ and $6.4x10^{-3}$ $\mu m^3/\mu m^2$.

4.3 Chemical analysis

Low-resolution XPS survey spectra of the analyzed samples reveal the presence of various elements on the surface, including C, Au, Cl, O, Si and N regardless of whether NH_3 is used during the deposition process. However, their atomic percentages notably vary (Table 2) . Additionally, trace levels of Na and K are detected (probably coming from the glass substrate). Note the presence of Si with a non-negligible surface atomic composition (Table 2), indicating a partial coverage of the glass substrate or its total coverage with a film of less than ~10 nm in thickness. Indeed, XPS is a surface analysis technique and provides chemical information on the outer surface layer without exceeding a sampling depth of 10 nm. Since the presence of Si is only due to the sample-glass substrate, it can be deduced that NH_3 gas prevents the formation of a continuous and/or thick NC film, in agreement with AFM observations performed on A sample (Figure 7b).

Table 2 : Surface chemical composition (at%) of A (with NH_3) and NA (without NH_3) samples determined by XPS.

Sample	C(%)	Au(%)	Cl(%)	O(%)	Si(%)	N(%)
A	36.0	3.5	9.5	31.7	10.7	8.2
NA	55.7	13.8	1.4	23.5	4.3	1.4

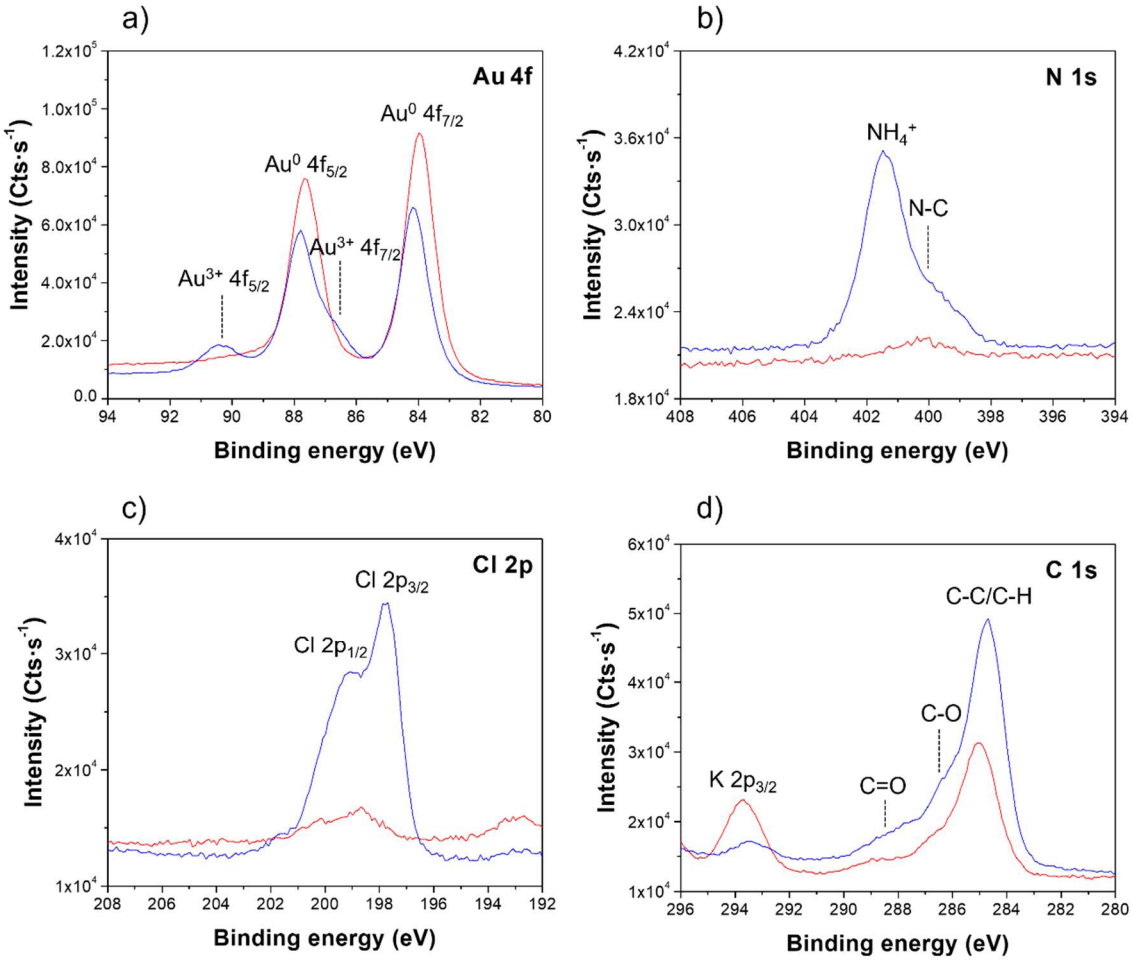

Figure 6 : High resolution XPS spectra of NC films prepared with (NA sample in red) and without (A sample in blue) NH_3 addition a) Au 4f, b) N 1s, c) Cl 2p and d) C 1s spectra

Table 2 also evidences a gold atomic percentage significantly higher in the NA sample, i.e. when ammonia is not used in the deposition process. High-resolution Au 4f XPS spectra in Figure 8a show that in both samples gold is mainly present in its metallic state (Au^0), therefore in the deposition process an effective reduction of the gold salt occurs leading to conversion of Au^{3+} to Au^0. In particular, the Au 4f spectrum of the NC film deposited without NH_3 appears dominated by the Au^0 contributions. The Au 4f spectrum of the NA sample consists of a doublet (Au $4f_{7/2}$ and Au $4f_{5/2}$, respectively, at 84.0 and 87.7 eV) due to spin-orbit coupling, the position being in agreement with previous literature on Au NPs[39], [40]. This seems to well correlate with optical characterization results and naked-eye observations. In fact, the greater amount of Au^0 in the film produced without NH_3 results in a red-purple plasmon resonance profile as a signature of gold NPs.

Even if the XPS fingerprint of metallic gold is identified for both samples[41], Au^{3+} contributions are also clearly present in the Au 4f spectrum of A sample (see assignments in Figure 8a), suggesting an uncomplete gold reduction when ammonia is added to the DBD feed mixture. Therefore, the introduction of NH_3 in the gas-phase during NC film processing promotes a decrease of the plasma reduction efficiency on the gold salt.

It is worth noting that the atomic concentrations of Cl and N are almost negligible in the NA sample (Table 2), contrary to the case of the A sample prepared with NH_3 addition. Indeed, the high-resolution N 1s spectrum of the NA sample exhibits the characteristic contributions of amino and ammonium groups at a binding energy of 399.8 and 401.7 eV respectively (Figure 8b)[42]. In parallel, the Cl 2p doublet peak of the NA sample with Cl $2p_{3/2}$ and Cl $2p_{1/2}$ components respectively at 197.8 eV and 199,0 eV, respectively, suggests the contribution from a chloride salt (Figure 8c)[42]. It is worth mentioning that in the case of the A sample, the presence of NH_4^+ (N 1s spectrum, Figure 8b) and metal chloride contributions (revealed by the Au^{3+} and Cl^- contributions in the Au 4f

and Cl 2p XPS spectra, respectively) point to the possible formation of NH_4AuCl_4 salt, reasonably occurring via acid-base reaction between $HAuCl_4$ and NH_3.

Both A and NA samples contains carbon (Table 2), meaning that with and without NH_3 the process leads to the formation of a carbon-based NC from isopropanol fragmentation and polymerization during the plasma discharge. The C atomic percentage is lower with NH_3, (Table 2) in this case it is not possible to exclude that graphite might be produced as suggested by the black color of A sample and the suspicion of graphite presence suggested by XRD analysis. The examination of the high-resolution C1s XPS spectra in Figure 8d shows that both of A and NA samples present contributions from C-H/C-C, C-O and C=O moieties. At this stage Raman spectroscopy is required to have a better knowledge of the carbon-containing component of the produced NC films.

Raman spectra (Figure 9) reveals a broad intensity region (1000 and 2000 cm^{-1}) ascribed to carbon-based species[43] and related to the polymer-like film formed during the plasma process. Furthermore, an intense peak at 287 cm^{-1} is also identified. According to Chang et *al.*[44] low frequency (<300 cm^{-1}) vibrational modes can be produced by interactions between gold surfaces and halide anions such as chloride (Cl^-), thus the presence of Au-Cl vibrational modes cannot be discarded in any of the deposited material. However, the presence of Au-Cl stretch mode at 339 cm^{-1}[45] and the stronger signal at lower frequency indicates that $[AuCl_4]^-$ species are also present maybe in the form of NH_4AuCl_4 salt. Once again the introduction of NH_3 into the plasma seem to decrease the $HAuCl_4$ reduction efficiency.

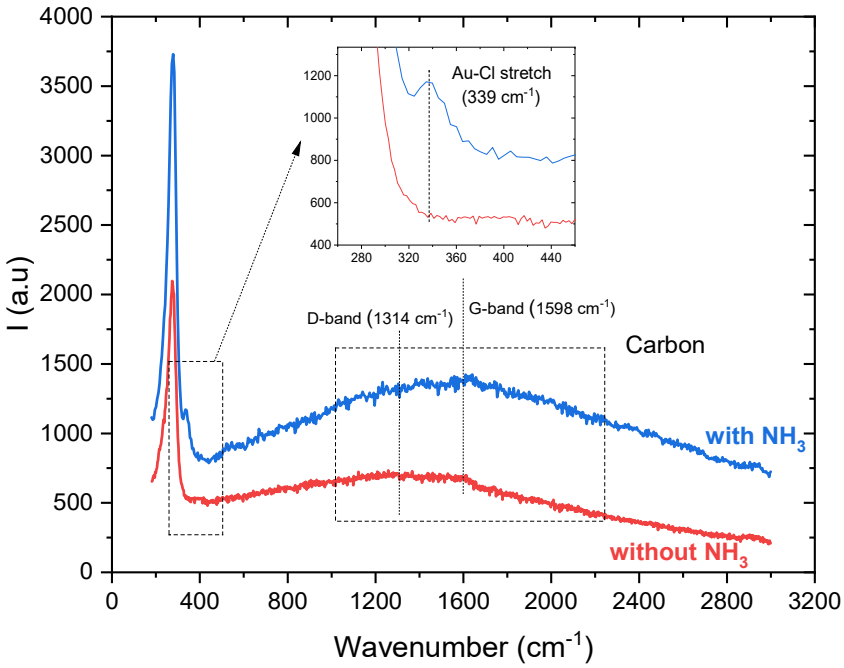

Figure 7 : Raman spectra of as-deposited Au NPs-based film.

To have information on the NPs chemical composition, SEM Z-contrast imaging and EDS mapping are performed. On NA sample (**Errore. L'origine riferimento non è stata trovata.**), contrast imaging on selected zones evidences more details on the composition of the previously observed NPs (Figure 10a). They appear as surrounded by a low electronic density matter like a polymer (Figure 10b). Chemical mapping confirms that the core of these NPs is made by metallic gold (the yellow highlighted areas are oxygen free) while the outer is gold free. This metallic core can be single of multiple as highlighted in Figure 10c. The whole NP volume appears chlorine and nitrogen free.

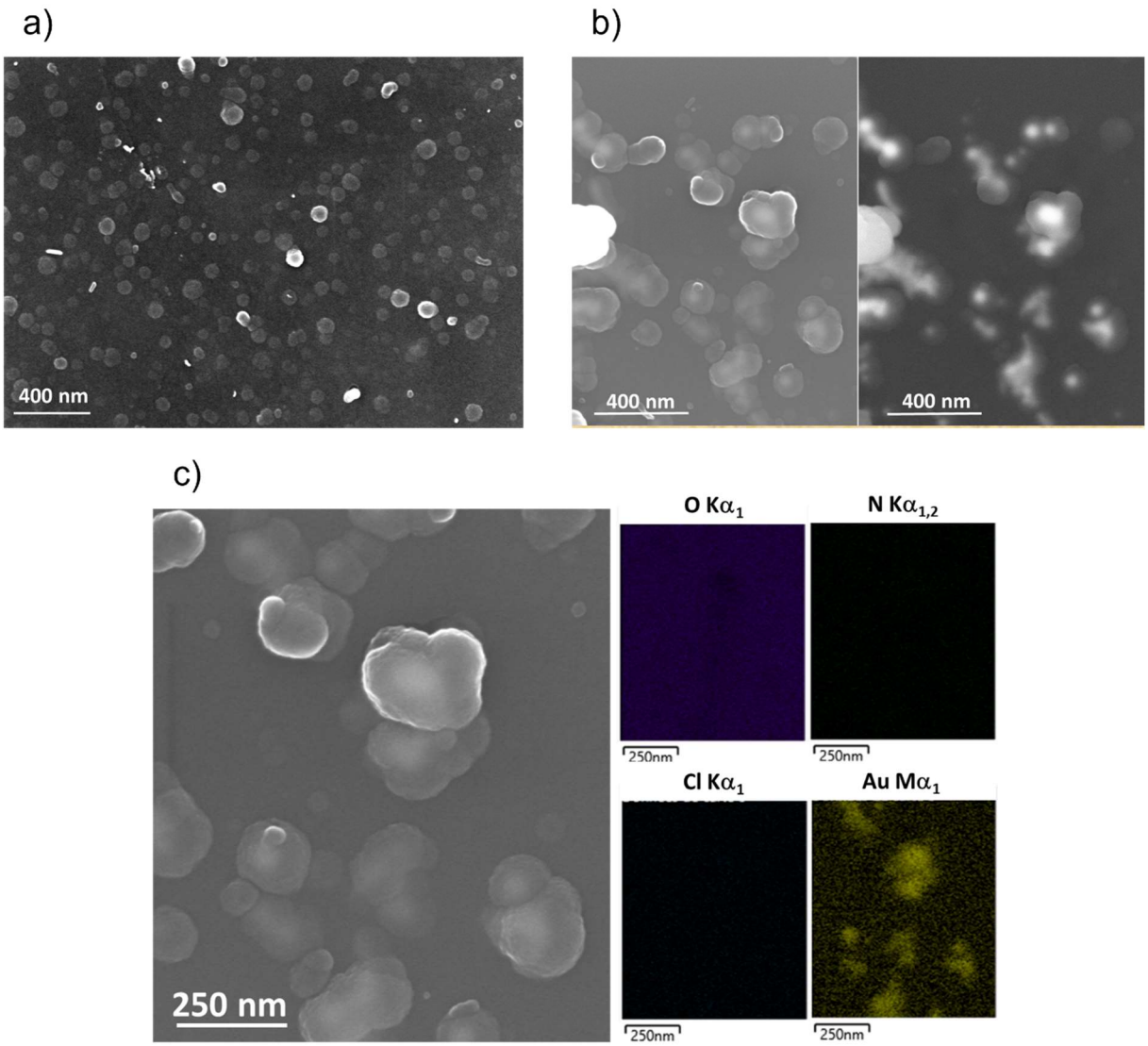

Figure 8 : SEM-EDS analysis of NA sample: a) SEM micrograph of an assembly of particles, b) Z-contrasting image highlighting the difference in the chemical composition of the inner and outer parts of the observed particles and c) Chemical mapping confirming the inorganic nature of the particle core (metallic gold) and the organic nature of its outer shell (probably oxygen and carbon)

An unambiguous conclusion cannot be done on the carbon-based chemical nature of the outer gold core layer in these NPs as carbon was pulverized everywhere to allows SEM analysis.

Samples with ammonia, coupled SEM and EDS results are fully different (

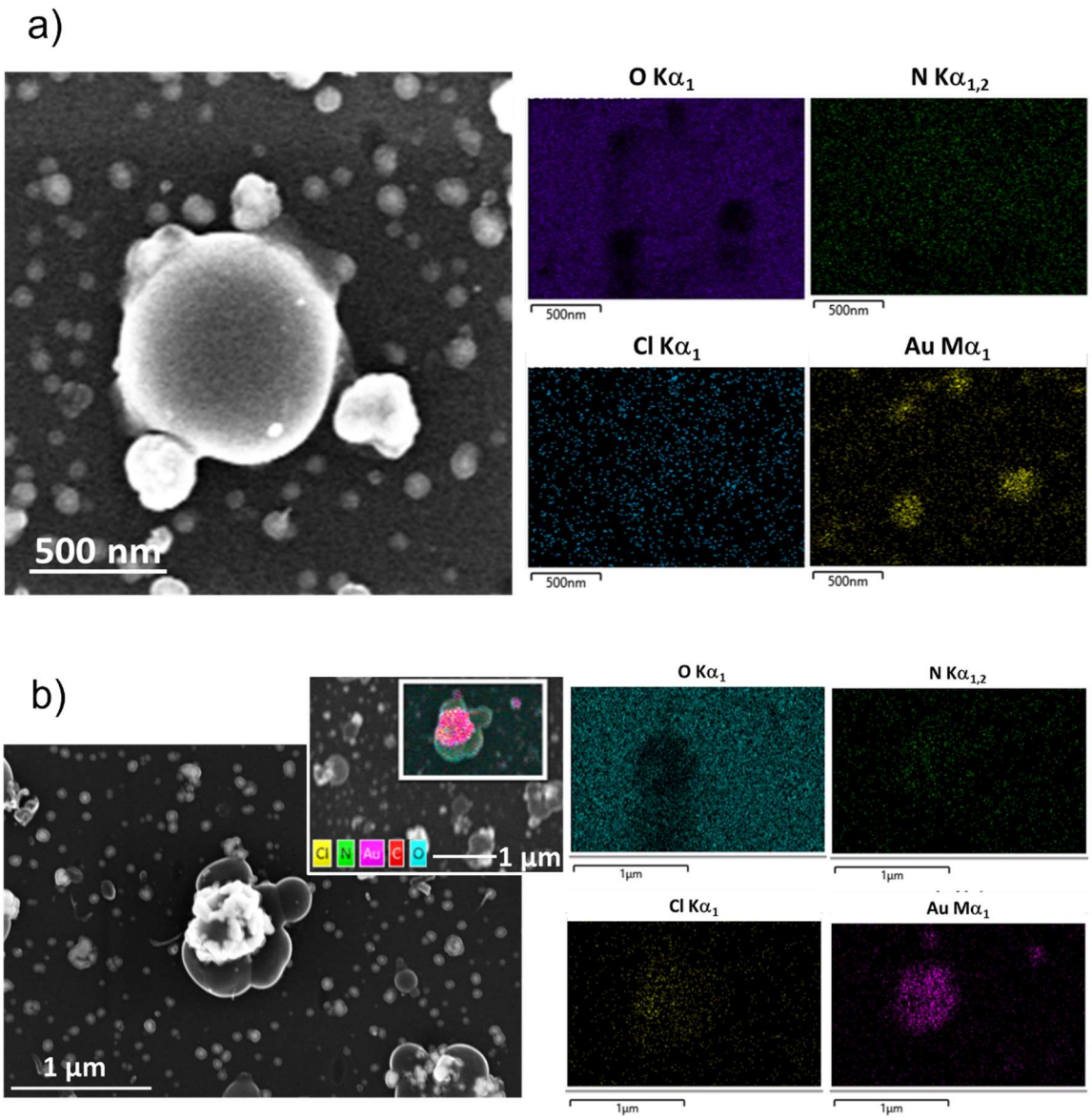

Figure 9), chemical mapping on such complex objects confirms that outer small particles are metallic gold particles, while the inner part is free from oxygen, and contain nitrogen and chlorine suggesting the formation of a kind of amorphous NH_4Cl and/or NH_4AuCl_4 salts, in agreement with the observation of Cl^-, $AuCl_4^-$, and NH_4^+ signatures in the high-resolution Cl 2p and Au 4f XPS spectra and that of ammonium groups in the N 1s one.

Beside these large objects, SEM images also evidence small and non-aggregated particles (

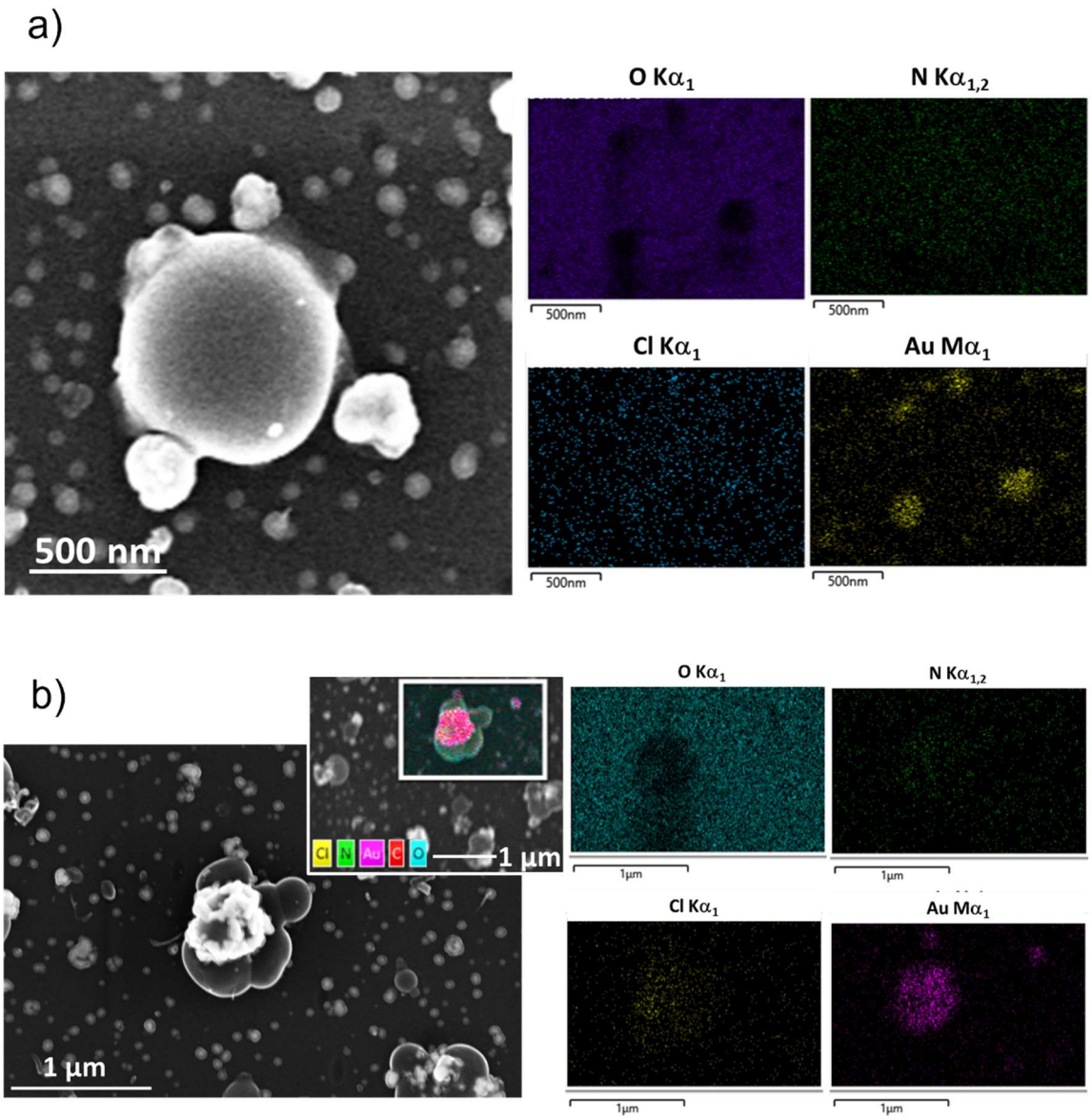

Figure 9). They seem to be of almost the same nature as those observed in sample NA, i.e. consisting of a metallic gold core surrounded by a kind of carbon-based soft matter. Non-coated small particles also appear on the collected images but as confirmed by EDS chemical mapping (not shown) they are only carbon made resulting from performed carbon pulverization treatment.

It can be therefore concluded that the chemical reactivity of NH_3 largely influences the salt reduction, furthermore, its concentration (133 ppm) small as compared to that of IPA (2%) and large compared to that of gold salt (about 6 ppm). Before discussing the different explanations, it is worth studying the influence of gas chemical composition on the plasma by optical emission spectroscopy.

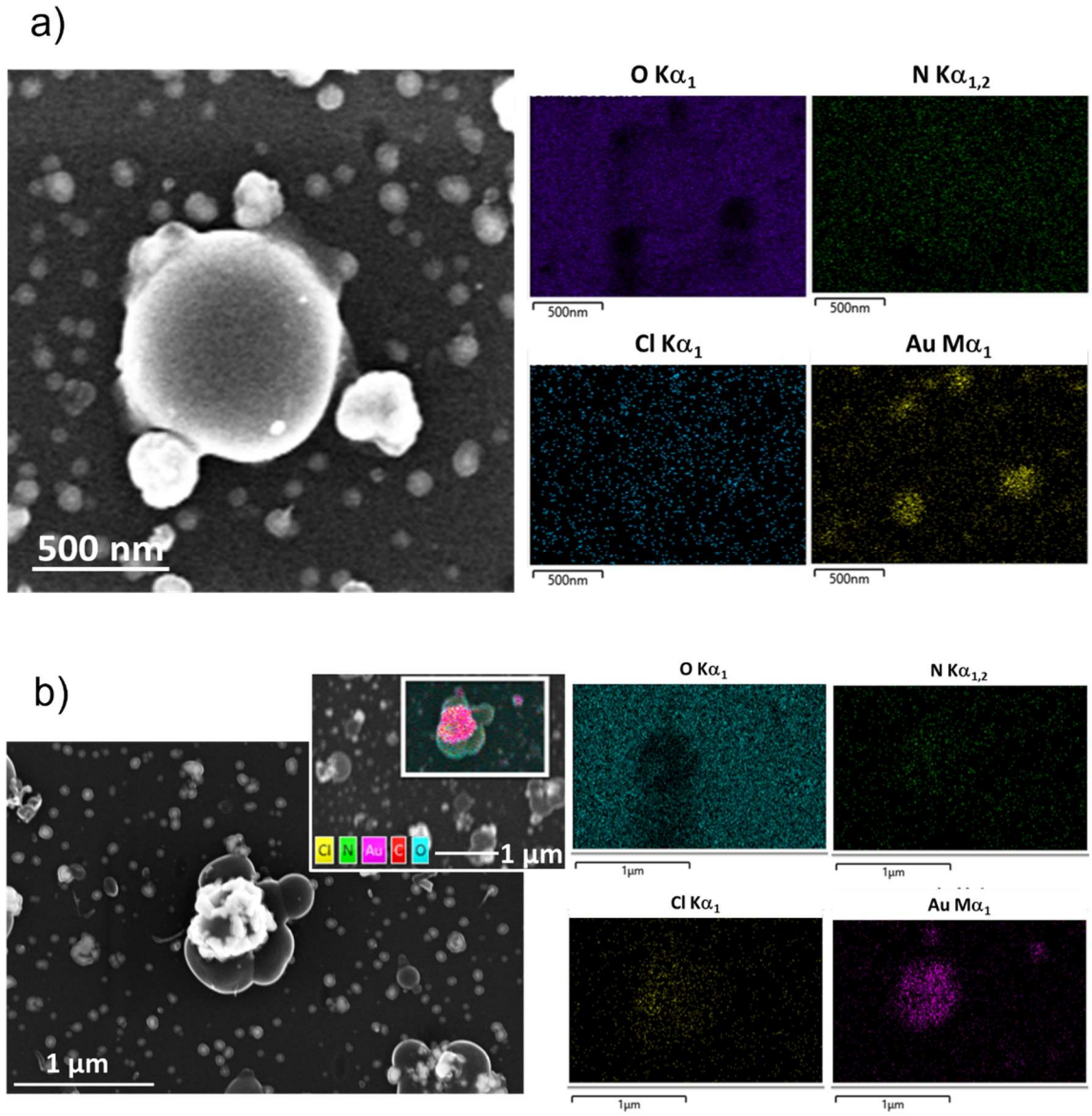

Figure 9.SEM- EDS chemical mapping of two representative particles of NA sample suggesting that their inner part is made from NH_4Cl or NH_4AuCl_4 while metallic gold nanoclusters concentrate in their outer part.

5 Plasma analysis

During the plasma deposition of Au-containing -NPs NC coatings, optical emission spectra were recorded. A typical spectrum in the 650-1000 nm range is presented in Figure 12a. It is important to highlight that regardless of the experimental condition, emitted radiation was dominated by deexcitation of Ar I levels (4p-4s transition). Interestingly, the addition of the 133 ppm of NH_3 into Ar/IPA discharge does not result in the emission of NH^* excited species (at 324 nm, $c^1\Pi \longrightarrow a^1\Delta$, 5.42 eV $\longrightarrow$1.55 eV) as it is observed in low frequency Ar/NH_3 DBDs[13]. The excitation of NH species typically occurs through collisions with electrons of energy close to 5 eV. Therefore, the absence of NH^* might be attributed to the lack of low-energy electrons, which instead could be colliding with isopropanol molecules which has a concentration of about 2%. These collisions lead to the breaking of C-H (4.28 eV), C-O (3.71 eV) and O-H (4.80 eV) bonds. This in turn leads to the IPA plasma polymerization, as suggested by XPS results. Nevertheless, emission lines corresponding to H_α and OH^* radicals (at 309 and 656 nm, respectively) are not observed, which suggests the absence or the very fast consumption of these radicals.

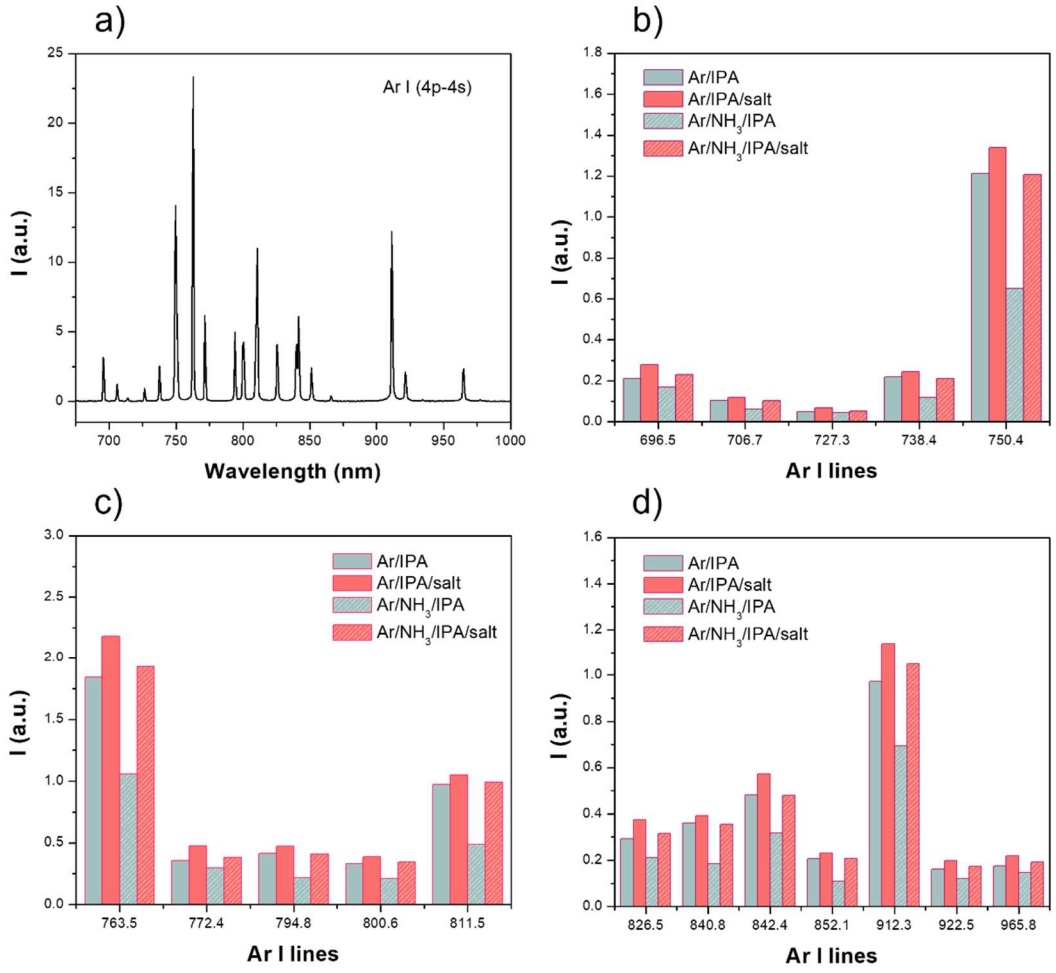

Figure 10: a) Typical optical emission spectrum of Ar/IPA/salt DBD b) c) and d) Ar I intensity lines in different wavelength ranges of Ar/IPA DBD with and without NH_3, and with and without gold salt.

It must be noted that the intensity emission of Ar I line varies depending on the gases and precursors introduced during the plasma process. Figure 12 reports the intensity of argon lines during the reduction and deposition of the gold salt with and without NH_3. The intensities are also compared when no salt is introduced to facilitate understanding of the process. The addition of IPA to Ar/NH_3 decreases the intensity of Ar emission, while the addition of the salt to Ar/IPA or to Ar/NH_3/IPA increases all the Ar emission lines. The decrease of Ar emission due to the addition of IPA vapors (IPA droplets are fully evaporated before the plasma inlet) could be related to the transition from the diffuse glow discharge to the localized filamentary discharge. The increase of Ar emission induced by the salt introduction could be explained by the fact that even if IPA mainly evaporates from the droplets between the atomizer and the plasma, according to the aerosol characterization, each droplet leads to a salt NP having a diameter of about 30 nm at the plasma entrance. These NPs should theoretically lead to Au NPs of about 12 nm in case of complete gold salt reduction and if they are dried but not reduced the salt crystal size is about 25 nm. All these particles are large enough to be charged by the plasma which induces a decrease in the electron density. This electron reduction is usually compensated by an increase of the electron energy, which is in agreement with the Ar emission increase as Ar4p is excited by high energy electrons [46].

A remarkable point is that the addition of $HAuCl_4$ salt to the Ar/NH_3/IPA plasma strongly increases the intensity of Ar I lines, so that the emission observed in the Ar/NH_3/IPA/salt process is nearly equal to that of Ar/IPA. This strong increase cannot be explained only by the presence of the NPs in the plasma, but is probably also associated to a decrease of the NH_3 proportion. Since NH_3 is added to the dilution flow, i.e. 400 ms before

entering the plasma reactor, this result suggests that NH_3 is partially consumed by a reaction with the salt, leading to the formation of a new component. This hypothesis will be further discussed in the next section.

6 Discussion and Conclusion

According to the NC thin film analysis, NH_3 addition drastically influences gold salt reduction:

- Without NH_3, in NA samples, gold salt appears almost fully reduced (XPS and EDS), leading to gold NPs of about 8 nm diameter according to XRD. These gold NPs have a large plasmonic resonance. The diameter of the NPs observed on the substrate are larger, about 12 nm according to AFM images. The gold NPs are probably covered by a thin polymer layer which increases their sticking coefficient to the glass substrate. Most of these NPs are non-aggregated. However, they tend to have a rosary organization which explains the plasmonic absorption extending from 500 to 900 nm.
- With NH_3, in A samples, according to XPS, the quantity of gold incorporated in the films is smaller, and part of it is not reduced. XRD still detects gold crystallites with a larger diameter than in NA samples (13 nm), but AFM and SEM measurements show that most of them are aggregated and often embedded in thick layers of carbon polymer, which may also contain graphite. Part of the aggregation could occur on the sample surface, since according to AFM analyzes the NPs are not round but like a dome. Hence, the absence of a plasmonic absorption of the film could be due to a combination of several factors. First, the quantity of gold NPs is very small. Second, the aggregation might induce a quenching of the plasmonic resonance. Indeed, it is known that the plasmonic resonance of gold nanospheres in solution undergoes a decrease, a broadening and a redshift as the NPs aggregate[36], [47]. Finally, the presence of a thick layer of light-absorbing polymer around the NPs might hide the absorption.

In the light of these considerations, the formation of the gold NPs from the droplets in absence of ammonia is first discussed. In solution, the gold salt is dissolved to give colored $Au^{III}Cl_4^-$ ions. Isopropanol being a mild reductor, it might react with these ions, leading to the formation of colorless $Au^{I}Cl_2^-$ ions. However, this reaction has been shown to be slow, especially when the gold salt concentration is low[48]. Accordingly, we observed a good stability with time of the prepared salt solutions if the latter are placed in an opaque to UV light bottle. After injection, the aerosol keeps protected from UV light until it enters the plasma reactor, so that the reduction of gold should not occur before the plasma.

As shown by the morphological and chemical analyses of the coatings, the gold salt is totally reduced in the plasma reactor to form gold NPs. The modal diameter of the gold NPs determined from XRD is around 8 nm, which suggests that each salt solution droplet converts into a gold NP. The reduction of Au^{3+} ions to Au^0 atoms and their aggregation to form metal NPs thus probably occur in the nanoparticles resulting from IPA evaporation (i.e. evaporation of IPA present in one droplet of aerosolized salt solution) forming a solid salt NP imperfectly crystallized with eventual traces of liquid isopropanol. Several mechanisms could be implied in the reduction: (i) free electrons of the plasma electrons could enter the wet crystals and directly reduce gold; (ii) the reduction process could be induced by reactive radicals formed by decomposition of IPA; (iii) the reduction may be driven by photochemical reduction resulting from the emission of vacuum ultraviolet light observed in dielectric barrier discharges (DBDs) in Ar[49], or by thermal decomposition.

Concerning the first two hypotheses, Vasudevan et al.[50] found that, using an atmospheric pressure plasma jet in an aqueous solution of $HAuCl_4$, the reduction of Au^{3+} ions and the subsequent deposition of gold NPs is primarily driven by the presence of free electrons within the plasma and the in-situ formation of hydrogen peroxide resulting from the combination of OH^* radicals. The participation of H^* and OH^* radicals is also reported in[51]. Nevertheless, this conclusion cannot be drawn with the evidence found under the experimental conditions of this research. According to UV-range spectrum (220-400 nm) of Ar/IPA/salt discharge, the emission of OH excited state is not observed. On the other hand, in this work, other reactive radicals might be generated by the decomposition of IPA, for instance the radical $\bullet C(CH_3)_2OH$, which is known to quickly reduce the Au^{3+} ions to Au^0 atoms[48], [52]. Note that these reactions involving electrons or radicals are slow if the droplets are completely dry at the entrance of the plasma, since the mobility in solid crystal salt is very low.

On the other hand, photochemical or thermal reduction of the Au^{3+} ions to Au^0 could be envisaged even in the solid phase. Indeed, $AuCl_4^-$ ions are known to be reduced to Au^0 atoms by UV light around 250 – 350 nm[53]. The formation of the NPs from the isolated Au^0 atoms is then generally obtained by annealing. However, under our experimental conditions, in the 250 – 350 nm range of the emitted plasma spectra, no emissions are found which suggests a limit influence of this reduction mechanism. However, in Ar DBD, there is an efficient continuum emission around 130 nm that largely contribute to secondary emission of the cathode as there is no auto-absorption of this emission due to Ar_2 dissociation. These photons which play a dominant role in the plasma physics [19] can also play a role in plasma chemistry. Besides, thermal direct synthesis of nanoparticles by decomposition of $HAuCl_4$ films at 150°C has also been reported [21]. However, such a temperature cannot be reached in a DBD plasma having a power of 0.5 W/cm^3.

Focusing on the effect of NH_3 on these mechanisms, as previously mentioned, plasma optical emission spectroscopy results suggest that ammonia reacts with the salt before entering the plasma reactor. Indeed, ammonia is a base and is known to react with $HAuCl_4$, leading to the formation of another salt, *e.g.* NH_4AuCl, or to amine gold complexes, such as 'fulminating gold'. These compounds may have a different solubility than HAuCl4, and distinct properties regarding the reduction of gold and the formation of NPs. For instance, in aqueous solution, the addition of ammonia is shown to reduce the size of the formed NPs[54], [55].

In this work, several hypotheses might explain the hindering effect of ammonia. First, the reaction of ammonia with the gold salt injected with residual liquid isopropanol may lead to the formation of a new gold salt less miscible with isopropanol, which could precipitate to form a dry crystal before entering the plasma cell. The plasma reduction of the salt would thus have to occur in the solid phase, so that only the photochemical and thermal mechanism could also occur. Ammonium ions may also act as electron scavengers reducing the salt reduction and the charge of the NPs and then their drift to the substrate. Another possibility, in the case NH_3 addition leads to a NPs size decrease as observed in aqueous solution, is that the gold NPs are too small to have a constant charge and thus to be electrostatically transported to the surface, which might also have an effect on the charging of nanoparticles, preventing their deposition.

7 Acknowledgments

The authors thank the Agence Nationale de la Recherche (ANR) for the financial support of the PLASSEL project (ANR-21-CE08-0038) and the SEAM Labex (ANR-11-LBX-086, ANR-11-IDEX-0502). R. Rincón was supported by the European Union-NextGenerationEU and the Spanish Ministerio de Universidades (Plan de Recuperacion, Transformación y Resiliencia).

8 References

[1] U. Kogelschatz, « Dielectric-Barrier Discharges: Their History, Discharge Physics, and Industrial Applications ».

[2] C.-P. Klages, K. Hopfner, N. Klake, et R. Thyen, « Surface Functionalization at Atmospheric Pressure by DBD-Based Pulsed Plasma Polymerization », *Plasmas and Polymers*, 2001.

[3] T. Sakoda, Y.-M. Sung, et K. Matsukuma, « Plasma treatment on electrode surfaces of bifacial silicon solar cells », *Solar Energy Materials and Solar Cells*, vol. 90, nº 7-8, p. 1089-1097, mai 2006, doi: 10.1016/j.solmat.2005.06.008.

[4] J. Lelièvre *et al.*, « Efficient silicon nitride SiN_x:H antireflective and passivation layers deposited by atmospheric pressure PECVD for silicon solar cells », *Prog Photovolt Res Appl*, vol. 27, nº 11, p. 1007-1019, nov. 2019, doi: 10.1002/pip.3141.

[5] F. Fanelli et F. Fracassi, « Thin Film Deposition on Open-Cell Foams by Atmospheric Pressure Dielectric Barrier Discharges », *Plasma Processes and Polymers*, vol. 13, nº 4, p. 470-479, 2016, doi: 10.1002/ppap.201500150.

[6] S. A. Starostin, M. Creatore, J. B. Bouwstra, M. C. M. van de Sanden, et H. W. de Vries, « Towards Roll-to-Roll Deposition of High Quality Moisture Barrier Films on Polymers by Atmospheric Pressure Plasma Assisted Process: Towards Roll-to-Roll Deposition of High Quality Moisture Barrier Films on Polymers by Atmospheric Pressure Plasma Assisted Process », *Plasma Process. Polym.*, vol. 12, nº 6, p. 545-554, juin 2015, doi: 10.1002/ppap.201400194.

[7] F. Massines, C. Sarra-Bournet, F. Fanelli, N. Naudé, et N. Gherardi, « Atmospheric Pressure Low Temperature Direct Plasma Technology: Status and Challenges for Thin Film Deposition », *Plasma Processes Polym.*, vol. 9, nº 11-12, p. 1041-1073, déc. 2012, doi: 10.1002/ppap.201200029.

[8] Y. P. Raizer, *Gas Discharge Physics*, 2nd éd. Springer Berlin, Heidelberg, 1991.

[9] U. Kogelschatz, B. Eliasson, et W. Egli, « From ozone generators to ¯at television screens: history and future potential of dielectric-barrier discharges », *Pure Appl. Chem.*, 1999.
[10] R. Brandenburg, « Dielectric barrier discharges: progress on plasma sources and on the understanding of regimes and single filaments », *Plasma Sources Sci. Technol.*, vol. 26, nº 5, p. 053001, mars 2017, doi: 10.1088/1361-6595/aa6426.
[11] F. Massines, N. Gherardi, N. Naudé, et P. Ségur, « Recent advances in the understanding of homogeneous dielectric barrier discharges », *Eur. Phys. J. Appl. Phys.*, vol. 47, nº 2, p. 22805, août 2009, doi: 10.1051/epjap/2009064.
[12] N. Osawa et Y. Yoshioka, « Generation of low-frequency homogeneous dielectric barrier discharge at atmospheric pressure », *IEEE Trans. Plasma Sci.*, vol. 40, nº 1, p. 2-8, janv. 2012, doi: 10.1109/TPS.2011.2172634.
[13] R. Bazinette, R. Subileau, J. Paillol, et F. Massines, « Identification of the different diffuse dielectric barrier discharges obtained between 50 kHz to 9 MHz in Ar/NH3at atmospheric pressure », *Plasma Sources Sci. Technol.*, vol. 23, nº 3, p. 035008, mai 2014, doi: 10.1088/0963-0252/23/3/035008.
[14] R. Magnan, G. Hagelaar, M. Chaker, et F. Massines, « Atmospheric pressure dual RF–LF frequency discharge: transition from α to α – γ -mode », *Plasma Sources Sci. Technol.*, vol. 30, nº 1, p. 015010, janv. 2021, doi: 10.1088/1361-6595/abd2ce.
[15] F. Fanelli, A. M. Mastrangelo, et F. Fracassi, « Aerosol-Assisted Atmospheric Cold Plasma Deposition and Characterization of Superhydrophobic Organic–Inorganic Nanocomposite Thin Films », *Langmuir*, vol. 30, nº 3, p. 857-865, janv. 2014, doi: 10.1021/la404755n.
[16] B. K. Kandola, « Nanocomposites », in *Fire Retardant Materials*, Elsevier, 2001, p. 204-219. doi: 10.1533/9781855737464.204.
[17] Weslley Rick Viana Sampaio, Petteson Linniker Carvalho Serra, Noelio Oliveira Dantas, Rômulo Ríbeiro Magalhães de Sousa, et Anielle Christine Almeida Silva, « Nanocomposites Thin Films: Manufacturing and Applications », in *Nanocomposite Materials for Biomedical and Energy Storage Applications*, Ashutosh Sharma, Éd., Rijeka: IntechOpen, 2022, p. Ch. 4. doi: 10.5772/intechopen.103961.
[18] M. A. Garcia, « Surface plasmons in metallic nanoparticles: fundamentals and applications », *J. Phys. D: Appl. Phys.*, vol. 45, nº 38, p. 389501, sept. 2012, doi: 10.1088/0022-3727/45/38/389501.
[19] A. Trügler, *Optical Properties of Metallic Nanoparticles*, vol. 232. in Springer Series in Materials Science, vol. 232. Cham: Springer International Publishing, 2016. doi: 10.1007/978-3-319-25074-8.
[20] V. Amendola, R. Pilot, M. Frasconi, O. M. Maragò, et M. A. Iatì, « Surface plasmon resonance in gold nanoparticles: a review », *J. Phys.: Condens. Matter*, vol. 29, nº 20, p. 203002, mai 2017, doi: 10.1088/1361-648X/aa60f3.
[21] K. L. Kelly, E. Coronado, L. L. Zhao, et G. C. Schatz, « The Optical Properties of Metal Nanoparticles: The Influence of Size, Shape, and Dielectric Environment », *J. Phys. Chem. B*, vol. 107, nº 3, p. 668-677, janv. 2003, doi: 10.1021/jp026731y.
[22] H. A. Atwater et A. Polman, « Plasmonics for improved photovoltaic devices », *Nature Mater*, vol. 9, nº 3, p. 205-213, mars 2010, doi: 10.1038/nmat2629.
[23] J. Profili, O. Levasseur, J.-B. Blaisot, A. Koronai, L. Stafford, et N. Gherardi, « Nebulization of Nanocolloidal Suspensions for the Growth of Nanocomposite Coatings in Dielectric Barrier Discharges: Nebulization of Nanocolloidal Suspensions… », *Plasma Process. Polym.*, vol. 13, nº 10, p. 981-989, oct. 2016, doi: 10.1002/ppap.201500223.
[24] P. Brunet, R. Rincón, Z. Matouk, M. Chaker, et F. Massines, « Tailored Waveform of Dielectric Barrier Discharge to Control Composite Thin Film Morphology », *Langmuir*, vol. 34, nº 5, p. 1865-1872, févr. 2018, doi: 10.1021/acs.langmuir.7b03563.
[25] A. Uricchio, E. Nadal, B. Plujat, G. Plantard, F. Massines, et F. Fanelli, « Low-temperature atmospheric pressure plasma deposition of TiO2-based nanocomposite coatings on open-cell polymer foams for photocatalytic water treatment », *Applied Surface Science*, vol. 561, p. 150014, sept. 2021, doi: 10.1016/j.apsusc.2021.150014.
[26] J. Profili, O. Levasseur, N. Naudé, C. Chaneac, L. Stafford, et N. Gherardi, « Influence of the voltage waveform during nanocomposite layer deposition by aerosol-assisted atmospheric pressure Townsend discharge », *Journal of Applied Physics*, vol. 120, nº 5, p. 053302, août 2016, doi: 10.1063/1.4959994.
[27] E. Nadal, N. Milaniak, H. Glenat, G. Laroche, et F. Massines, « A new approach for synthesizing plasmonic polymer nanocomposite thin films by combining a gold salt aerosol and an atmospheric pressure low-temperature plasma », *Nanotechnology*, vol. 32, nº 17, p. 175601, févr. 2021, doi: 10.1088/1361-6528/abdd60.
[28] S. Porel, N. Venkatram, D. Narayana Rao, et T. P. Radhakrishnan, « *In Situ* Synthesis of Metal Nanoparticles in Polymer Matrix and Their Optical Limiting Applications », *j nanosci nanotechnol*, vol. 7, nº 6, p. 1887-1892, juin 2007, doi: 10.1166/jnn.2007.736.

[29] P. Brunet *et al.*, « Control of composite thin film made in an Ar/isopropanol/TiO_2 nanoparticles dielectric barrier discharge by the excitation frequency », *Plasma Process Polym*, vol. 14, nº 12, p. 1700049, déc. 2017, doi: 10.1002/ppap.201700049.
[30] N. Jidenko, C. Jimenez, F. Massines, et J.-P. Borra, « Nano-particle size-dependent charging and electro-deposition in dielectric barrier discharges at atmospheric pressure for thin SiO_x film deposition », *J. Phys. D: Appl. Phys.*, vol. 40, nº 14, p. 4155-4163, juill. 2007, doi: 10.1088/0022-3727/40/14/009.
[31] J. Vallade, R. Bazinette, L. Gaudy, et F. Massines, « Effect of glow DBD modulation on gas and thin film chemical composition: case of Ar/SiH_4/NH_3 mixture », *J. Phys. D: Appl. Phys.*, vol. 47, nº 22, p. 224006, juin 2014, doi: 10.1088/0022-3727/47/22/224006.
[32] N. Milaniak, G. Laroche, et F. Massines, « Atmospheric-pressure plasma-enhanced chemical vapor deposition of nanocomposite thin films from ethyl lactate and silica nanoparticles », *Plasma Process Polym*, vol. 18, nº 2, p. 2000153, févr. 2021, doi: 10.1002/ppap.202000153.
[33] R. Bazinette, N. Sadeghi, et F. Massines, « Dual frequency DBD: influence of the amplitude and the frequency of applied voltages on glow, Townsend and radiofrequency DBDs », *Plasma Sources Sci. Technol.*, vol. 29, nº 9, p. 095010, sept. 2020, doi: 10.1088/1361-6595/ab8686.
[34] W. M. Haynes, Éd., *Handbook of Chemistry and Physics*, 0 éd. CRC Press, 2014. doi: 10.1201/b17118.
[35] M. J. H.-S. Toivo T. Kodas, « Aerosol Processing of Materials », *J. Am. Chem. Soc.*, 1999, doi: 10.1021/ja995709o.
[36] N. K. Kwon, T. K. Lee, S. K. Kwak, et S. Y. Kim, « Aggregation-Driven Controllable Plasmonic Transition of Silica-Coated Gold Nanoparticles with Temperature-Dependent Polymer–Nanoparticle Interactions for Potential Applications in Optoelectronic Devices », *ACS Appl. Mater. Interfaces*, vol. 9, nº 45, p. 39688-39698, nov. 2017, doi: 10.1021/acsami.7b13123.
[37] J. S. Villarrubia, « Algorithms for scanned probe microscope image simulation, surface reconstruction, and tip estimation », *J. Res. Natl. Inst. Stand. Technol.*, vol. 102, nº 4, p. 425, juill. 1997, doi: 10.6028/jres.102.030.
[38] D. J. Whitehouse, *Handbook of Surface and Nanometrology*, 0 éd. Taylor & Francis, 2002. doi: 10.1201/9781420034196.
[39] J. Xie, J. Y. Lee, et D. I. C. Wang, « Synthesis of Single-Crystalline Gold Nanoplates in Aqueous Solutions through Biomineralization by Serum Albumin Protein », *J. Phys. Chem. C*, vol. 111, nº 28, p. 10226-10232, juill. 2007, doi: 10.1021/jp0719715.
[40] M. P. Casaletto, A. Longo, A. Martorana, A. Prestianni, et A. M. Venezia, « XPS study of supported gold catalysts: the role of Au0 and Au+δ species as active sites », *Surf. Interface Anal.*, vol. 38, nº 4, p. 215-218, avr. 2006, doi: 10.1002/sia.2180.
[41] T. Darrah Thomas et P. Weightman, « Valence electronic structure of AuZn and AuMg alloys derived from a new way of analyzing Auger-parameter shifts », *Phys. Rev. B*, vol. 33, nº 8, p. 5406-5413, avr. 1986, doi: 10.1103/PhysRevB.33.5406.
[42] A. Galtayries, E. Laksono, J.-M. Siffre, C. Argile, et P. Marcus, « XPS study of the adsorption of NH3 on nickel oxide on Ni(111) », *Surf. Interface Anal.*, vol. 30, nº 1, p. 140-144, août 2000, doi: 10.1002/1096-9918(200008)30:1<140::AID-SIA820>3.0.CO;2-5.
[43] Z. Li, L. Deng, I. A. Kinloch, et R. J. Young, « Raman spectroscopy of carbon materials and their composites: Graphene, nanotubes and fibres », *Progress in Materials Science*, vol. 135, p. 101089, juin 2023, doi: 10.1016/j.pmatsci.2023.101089.
[44] M. Y. Chan, W. Leng, et P. J. Vikesland, « Surface-Enhanced Raman Spectroscopy Characterization of Salt-Induced Aggregation of Gold Nanoparticles », *ChemPhysChem*, vol. 19, nº 1, p. 24-28, janv. 2018, doi: 10.1002/cphc.201700798.
[45] P. J. Murphy et M. S. LaGrange, « Raman spectroscopy of gold chloro-hydroxy speciation in fluids at ambient temperature and pressure: a re-evaluation of the effects of pH and chloride concentration », *Geochimica et Cosmochimica Acta*, vol. 62, nº 21-22, p. 3515-3526, nov. 1998, doi: 10.1016/S0016-7037(98)00246-4.
[46] R. Bazinette, J. Paillol, et F. Massines, « Optical emission spectroscopy of glow, Townsend-like and radiofrequency DBDs in an Ar/NH_3 mixture », *Plasma Sources Sci. Technol.*, vol. 24, nº 5, p. 055021, sept. 2015, doi: 10.1088/0963-0252/24/5/055021.
[47] N. J. Halas, S. Lal, W.-S. Chang, S. Link, et P. Nordlander, « Plasmons in Strongly Coupled Metallic Nanostructures », *Chem. Rev.*, vol. 111, nº 6, p. 3913-3961, juin 2011, doi: 10.1021/cr200061k.
[48] B. Pal, P. K. Sen, et K. K. Sen Gupta, « Reactivity of alkanols and aryl alcohols towards tetrachloroaurate(III) in sodium acetate-acetic acid buffer medium », *J. Phys. Org. Chem.*, vol. 14, nº 5, p. 284-294, mai 2001, doi: 10.1002/poc.361.
[49] R. Robert, G. Hagelaar, N. Sadeghi, R. Magnan, L. Stafford, et F. Massines, « Role of excimer formation and induced photoemission on the Ar metastable kinetics in atmospheric pressure Ar–NH_3 dielectric barrier

discharges », *Plasma Sources Sci. Technol.*, vol. 31, nº 6, p. 065010, juin 2022, doi: 10.1088/1361-6595/ac7748.
[50] A. Vasudevan *et al.*, « From faceted nanoparticles to nanostructured thin film by plasma-jet redox reaction of ionic gold », *Journal of Alloys and Compounds*, vol. 928, p. 167155, déc. 2022, doi: 10.1016/j.jallcom.2022.167155.
[51] K. Nitta, Y. Shimizu, K. Terashima, et T. Ito, « Plasma-assisted synthesis of size-controlled monodisperse submicron gold particles using inkjet droplets », *J. Phys. D: Appl. Phys.*, vol. 54, nº 33, p. 33LT01, août 2021, doi: 10.1088/1361-6463/ac02f8.
[52] E. Gachard, H. Remita, J. Khatouri, B. Keita, L. Nadjo, et and J. Belloni, « Radiation-induced and chemical formation of gold clusters », *New J. Chem.*, vol. 22, nº 11, p. 1257-1265, 1998, doi: 10.1039/a804445g.
[53] M. Grzelczak et L. M. Liz-Marzán, « The relevance of light in the formation of colloidal metal nanoparticles », *Chem. Soc. Rev.*, vol. 43, nº 7, p. 2089-2097, 2014, doi: 10.1039/C3CS60256G.
[54] L. Delannoy, N. El Hassan, A. Musi, N. N. Le To, J.-M. Krafft, et C. Louis, « Preparation of Supported Gold Nanoparticles by a Modified Incipient Wetness Impregnation Method », *J. Phys. Chem. B*, vol. 110, nº 45, p. 22471-22478, nov. 2006, doi: 10.1021/jp062130l.
[55] F. Somodi *et al.*, « Modified preparation method for highly active Au/SiO2 catalysts used in CO oxidation », *Applied Catalysis A: General*, vol. 347, nº 2, p. 216-222, sept. 2008, doi: 10.1016/j.apcata.2008.06.017.